

A quantitative approach to understanding dated dune stratigraphies

Journal:	<i>Earth Surface Processes and Landforms</i>
Manuscript ID:	ESP-13-0109.R1
Wiley - Manuscript type:	Paper
Date Submitted by the Author:	n/a
Complete List of Authors:	Bailey, Richard; University of Oxford, School of Geography and the Environment Thomas, David; University of Oxford, School of Geography and Environment
Keywords:	drylands, dune, stratigraphy, dating, model

SCHOLARONE™
Manuscripts

Review

1

2

3

41A quantitative approach to understanding dated dune stratigraphies

5

62

7

83

9R.M. Bailey & D.S.G. Thomas

10

114

12

13

145

15

16

17

18

19

20

21

22

23

24

25

26

27

28

29

30

31

32

33

34

35

36

37

38

39

40

41

42

43

44

45

46

47

48

49

50

51

52

53

54

55

56

57

58

59

60

26

School of Geography and the Environment, University of Oxford

6

Abstract

7

8

9

10

11

12

13

14

15

16

17

18

19

20

21

22

23

24

25

26

27

28

29

30

31

32

33

34

35

36

37

38

39

40

41

42

43

44

45

46

47

48

49

50

51

52

53

54

55

56

57

58

59

60

26

Attempts to reconstruct past changes in climate-related forcing of dryland landscapes are hampered by the lack of an adequate quantitative framework for understanding the production and interpretation of dated sedimentary records. In drylands, as in other environments, information on past forcing conditions is progressively modified, degraded and removed from the available stratigraphic record by a series of ‘filters’ involving changes in the primary forcing factors themselves, geomorphological processes and the sampling/dating procedures. In this paper we describe a quantitative model that includes these effects, and use the model to examine the nature of preserved dryland sedimentary records and their relationships to primary forcing conditions: thicker preserved sedimentary records reflect periods of more intense aeolian activity; localized switching between erosion and deposition results in discontinuous and highly variable stratigraphic sequences; a preservation bias towards younger deposits is observed, potentially leading to a continuum of accumulation that decays approximately in proportion to $1/\sqrt{age}$. Time periods not represented by deposition can in some cases be interpreted as periods of higher precipitation and/or lower wind energy. An asymmetry exists between the efficiency with which past ‘drier’ and ‘wetter’ episodes can be identified, which relates to the time-separation of depositional periods and the correct distinction between hiatuses due to forcing conditions and those due to under-sampling. Relevant to this is the effect of random dating errors (statistical uncertainty), which (increasingly which age) filter-out higher

frequency events from the record. A new data treatment method (termed *Accumulation Rate Variability*) provides an efficient proxy for accumulation rates, and therefore the intensity of aeolian activity, with significant improvements over existing date-frequency methods. The filtering problem discussed applies to all attempts at understanding the timing and nature of past events, independent of the proxies and dating methods employed. Further explicit analysis of these issues would be beneficial.

Introduction

The erosion, (re-)deposition and preservation of aeolian dunes over Quaternary timescales is controlled directly and indirectly by several key factors, including wind energy (Fryberger, 1979), sediment moisture content, including effects on plant cover (Wolfe and Nickling, 1993) and sediment availability (Kocurek and Lancaster, 1999). Today about 20% of the World's drylands are covered by dunes, with these landforms extending into neighbouring areas where conditions are not presently conducive to aeolian sediment transport and dune activity. Controls on wind-blown sediment movement have evidently changed significantly over time.

With the capacity to establish the age of aeolian sediments through luminescence dating (Singhvi and Porat, 2008), dunes have become a significant component of Quaternary palaeoenvironmental research, especially in contexts where other (usually biological) proxies are lacking (Thomas and Burrough, 2012). It has recently been noted, however, that dunefields present several significant challenges for palaeoenvironmental and palaeoclimatic investigations (Thomas, 2013), including understanding the contexts of sediment preservation (Munyikwa, 2005), what controls the ages of the dune sediments that are preserved (Stone and Thomas, 2008), and how best to interpret dated dune records (Chase, 2009). There is, therefore, much still to be learned about how to interpret age/depth data from dune luminescence dating studies,

1
2
3
4
5
6
7
8
9
10
11
12
13
14
15
16
17
18
19
20
21
22
23
24
25
26
27
28
29
30
31
32
33
34
35
36
37
38
39
40
41
42
43
44
45
46
47
48
49
50
51
52
53
54
55
56
57
58
59
60

in terms of driving factors and sedimentary responses. This is particularly relevant as studies in other environmental contexts show the thickness of accumulated sediments to change over time (Tipper, 1983), as well as the relationship between bed thickness and time to be non-linear, with implications for how temporal processes are recorded in the sedimentary record (Kemp, 2012) . Two related questions therefore provide the impetus for the analysis in this paper: 1) from which periods of change in the key forcing factors is preserved dune sediment expected to date, and 2) when interrogating (through sampling and dating) the dune record, which environmental forcings might we expect to see represented by accumulated and preserved sediments, and which might we expect to miss?

Sediment preservation and the completeness of the stratigraphic record has long been a significant theme in the earth sciences (e.g. Barrell 1917), with a quantitative understanding important for debates involving evolution and the timing of extinctions (Anders *et al.*, 1987), astronomical forcing (Kemp 2012), and the role of time in preservation potential (Sadler, 1981). Breaks in sedimentary sequences, regardless of the mode of deposition, are to be expected, and occur at a range of temporal and spatial scales (Reineck, 1960), as shown through the application of a simple stochastic model (Tipper, 1983). Empirical analysis of tens of thousands of accumulation rate records (Sadler, 1981, Kemp, 2012) has demonstrated that accumulation rates scale inversely to the length of time over which records are measured, because longer time spans incorporate more and longer hiatuses in accumulation. Indeed, a total accumulation should not be expected, even for short time intervals, because all a record requires for a depositional phase to be recorded is *some* sediment from that phase to accumulate and not to be subsequently eroded (Sadler and Strauss, 1990). Sadler's (1981) analysis therefore implies that a 'complete' sedimentary record will

possess gaps, but so long as no gap exceeds or is equal to the duration of observation, a record should be deemed 'complete' (Kemp 2012).

The 'completeness' of dune records is currently a source of significant debate in palaeoenvironmental studies (Munyikwa, 2005, Thomas and Burrough, 2012). Correct interpretation of dune deposits requires an improved understanding of how ages relate to dune deposition and sediment preservation (Munyikwa, 2005; Stone and Thomas, 2008; Chase, 2009; Lomax *et al.*, 2011). A useful exercise is to regard the problem as one of progressive filtering of information from the initial climate forcing, through geomorphological response, to sediment deposition, sediment preservation, and ultimately, sampling for dating and subsequent interpretation (Figure 1). The information on climatic conditions available at the time of sediment deposition is modified, depleted and incompletely recorded over time by physical processes, and a key goal of this paper is to explicitly model and assess this process.

Kocurek (1998) addressed the difficulty of linking forcing factors to dune response conceptually, with a diagrammatic model that sought to explain the way that sediment system behaviour might interact with simple wet-dry climate changes, resulting in preservation of Saharan aeolian deposits. His model addresses how sediment supply (to a dune system) and sediment availability (for dune construction) is impacted by both wind energy variations and humid-arid transitions: without the arrival of new sediment from outside the dune system, arid, windy conditions would result in dune erosion; with new sediment becoming available (supplied for example by fluvial/slope wash inputs as aridity progressed), erosion would be succeeded by net dune accumulation. Dune systems might therefore experience both destructive and constructive phases associated with a propensity towards aeolian sediment transport, with the balances and temporal relationships between these phases affecting the likelihood and amount of net accumulation.

1
2
3
4 104 Telfer *et al.* (2010) developed this theme, introducing, in a probabilistic model,
5
6 105 feedbacks that represent the interactions between climatic and dune surface process
7
8 106 controls on sediment transport and deposition on a (linear) dune crest. The dune crest
9
10 107 was the morphological point of interest because it represents the location of maximum
11
12 108 dune height (and therefore greatest sediment accumulation in dune cross profiles) and
13
14 109 is the location where sampling for linear dune dating usually occurs. Multiple model
15
16 110 runs with differing external forcing scenarios predicted that sediment accumulation
17
18 111 along a dune crest might vary spatially, with marked implications for empirical sampling
19
20 112 strategies aimed at reconstructing Quaternary dune histories. A goal of this paper is to
21
22 113 develop a more generalized and largely physically-based model of the processes
23
24 114 controlling dune accumulation and preservation under scenarios which are linked
25
26 115 explicitly to annual precipitation and windspeed distribution. This in turn leads to an
27
28 116 explicit assessment of how confidently dated dune records can be interpreted as
29
30 117 climate proxies.
31
32
33
34
35
36
37
38

39 119 ***Aim and model description***

40
41 120 The purpose of the present modelling is to capture the net effects of a diverse range of
42
43 121 processes driving sand transport, accumulation and preservation over extended periods
44
45 122 (years to centuries), in the context of desert environments that extend over spatial
46
47 123 scales of 10^2 - 10^5 km². We reduce the problem to a 1D case, simulating changes in
48
49 124 surface height, through the net effect of erosion and deposition, over time periods
50
51 125 extending up to 10^5 years (within the range of Optically Stimulated Luminescence
52
53 126 (OSL) dating).
54
55
56
57 127 Key parameters controlling the balance of erosion/deposition in this model are:
58
59 128 windspeed (greater windspeeds raise sediment transport rates, potentially increasing
60
129 both erosion and deposition rates); precipitation (higher precipitation levels retard

erosion), and the relative size of 'external' sediment sources. We aim to produce a description of how sediment flux depends on basic relevant environmental parameters and as a starting point we consider equilibrium (aeolian) sediment flux and its dependence on windspeed.

Calculation of dry sediment flux

The amount of sediment entrained from a horizontal sand surface depends primarily on incident windspeed and the grain size of the material. Here, the various physical processes involved in entrainment and transport (for in-depth discussion see Duran et al., 2011; Wiggs, 2011) are not explicitly modelled and the sand flux (in units kg/m/s) is calculated, as a function of windspeed, using the semi-empirical relationship given in Equation 1 (reformulated from Dong et al., 2003):

$$q(u) = (c_1 + (c_2 d/D))^{-1} (1 - (v_T/u))^2 (u^3 \rho/g) \quad (\text{Eq. 1})$$

where $c_1=475.24$ and $c_2=93.62$ are fitted constants; d is grain size (here $d=200 \mu\text{m}$) and D is a reference grain size ($D=250 \mu\text{m}$), u is windspeed (m/s), g is acceleration due to gravity ($g=9.81 \text{ m/s}^2$) and ρ is the density of air ($\rho=1.25 \text{ kg.m}^{-3}$). The threshold velocity for entrainment (v_T) is interpolated from the data of Dong et al. (2003) shown in the inset to Figure 2. Example numerical solutions of q are shown in Figure 2 for windspeeds in the range 0-15 m/s, for three different grain sizes (150, 200 and 250 μm). To calculate potential sediment flux per year (Q), q should be multiplied by a factor t_{si} which is the number of seconds the wind blows at speed u_i , where the index denotes discrete windspeeds present in the annual windspeed distribution (this model is not spatially explicit and therefore wind direction is ignored):

$$Q = \sum_i (t_{si} q(u_i)) \quad (\text{Eq. 2})$$

The distribution of windspeed in many dryland areas has been observed to broadly follow a Weibull distribution (e.g. Merzouk, 2000; Zhang *et al.*, 2002; Flores-Aqueveque *et al.*, 2012) and we use this form in the present model. However, to reduce the computational expense of calculating sediment flux for each second of each simulated year, we use an 'effective windspeed' (u_{eff}). This is the windspeed which yields a flux, which when multiplied by an 'effective time' (t_{eff}) yields the same total sediment flux as that obtained by summing the flux due to windspeeds randomly selected from a Weibull distribution for the period of one year.

The choice of t_{eff} is to some extent arbitrary, but best chosen such that, (i) u_{eff} is not greater than the maximum value for which empirical data provides reliable estimates of mass flux (here 15 m/s; Figure 2) ($u_{eff} \rightarrow \infty$ as $t_{eff} \rightarrow 0$); (ii) u_{eff} is not a vanishingly small amount greater than the threshold velocity (v_t), such that numerical error becomes significant ($(u_{eff} - v_t) \rightarrow 0$ as $t_{eff} \rightarrow \infty$). We chose t_{eff} to be 2/3rds of one year ($t_{eff}=2.1024e7$ s), and calculated u_{eff} numerically as being that which satisfied $\min(|Q_w - t_{eff} Q(u_{eff})|)$, where Q_w is the sum (over 1 year) of 1 second flux calculations for windspeed (u) taken randomly from a Weibull distribution ($u \sim W(\lambda, k)$), where $P(u) = (k/\lambda)(u/\lambda)^{k-1} \exp(-(u/\lambda)^k)$. Three Weibull distributions are shown in Figure 3(i), spanning what we consider to range from 'low' to 'high' wind energy regimes; the vertical dashed line indicates the threshold velocity for entrainment of 200 μm grains. For each of these distributions, $\lambda=1.5$, and $k=2, 3.5, 5$ for low/medium/high scenarios respectively. Part (ii) of Figure 3 shows the distribution of sand flux (Q) resulting from each windspeed distribution (the result of drawing random windspeeds from each distribution and summing the flux over a 1 year period). Figure 3(iii) shows the effective windspeed u_{eff} versus k over a relevant range, with the threshold velocity

shown for reference (dashed horizontal line). The potential annual dry sediment flux, Q , is thus defined

$$Q = t_{eff}q(u_{eff}) \quad (\text{Eq.3})$$

We refer to Q as the *potential* annual dry flux because in reality a host of moisture-related factors exist which reduce the amount of sediment available for transport and these are discussed in the following sections.

Because in reality the distribution of windspeed does not remain identical from year to year, u_{eff} is varied randomly through time as the model runs (t_{eff} is kept constant), and in most cases presented in the following sections $u_{eff} \sim N(\mu_{u_{eff}} = 7, \sigma_{u_{eff}} = 1)$, as indicated in Figure 3(ii). So, u_{eff} is a small amount above the threshold velocity ($v_T = 6.4$ m/s), with the probability of both relatively windy and calmer years symmetrically distributed, as shown. Both the mean and standard deviation of u_{eff} can of course be varied through the simulation, and such scenarios are discussed in later sections. As noted above, precipitation plays an important and variable role in modulating sand flux, and relevant effects are described in the following section.

The effect of local moisture

Moisture has the effect of retarding sediment mobilization, both through the direct effect of cohesion and also the indirect effect of encouraging the formation of soil crusts, growth of vegetation, and ultimately soil formation. We parameterize these combined effects of moisture using a simple empirically-based relationship involving the values p (annual precipitation), p_0 (the threshold value below which annual precipitation has effectively no influence on sediment transport) and p_1 (the annual precipitation value above which effectively no sediment transport occurs):

202
$$k_m = \begin{cases} 1, & p < p_0 \\ 0, & p > p_1 \\ 1 + (p - p_0)(-1/(p_1 - p_0)), & p_0 \leq p \leq p_1 \end{cases} \quad (\text{Eq.4a,b,c})$$

203 Solutions for k_m are shown in Figure 4(i). We chose $p_0=150 \text{ mm yr}^{-1}$ and $p_1=500 \text{ mm yr}^{-1}$
204 based on both empirical observations of present-day precipitation and sediment mobility
205 indices under quasi-equilibrium conditions (e.g. Thomas *et al.*, 2005) and on
206 established landscape classifications for hyperarid to semiarid areas and their
207 precipitation associations (e.g. UNEP 1998). The straight line between p_0 and p_1
208 represents the most parsimonious parameterization of the observable (but unquantified)
209 gradient of aeolian activity between the two extremes. The annual sediment flux,
210 including moisture effects, is then defined

211
$$Q_m = k_m Q \quad (\text{Eq.5})$$

212 The combined effects of effective windspeed and precipitation on the sediment
213 transport rate (the potential for erosion/deposition, and hence the level of activity at the
214 surface) is shown graphically in Figure 4(ii) (further discussion below).

215 As in the case of windspeed (discussed above), precipitation in dryland areas is highly
216 variable from year to year (Hulme, 1996; Thomas, 2011), with for example mean
217 interannual variability in parts of the Kalahari and Sahara of 45% and 70% respectively
218 (Thomas and Shaw, 1991; Goudie, 2002). In the model this annual variability, as for
219 windspeed, is simulated by drawing random values from a Normal distribution:
220 $p \sim N(\mu_p, \sigma_p)$, where μ_p and σ_p can also be functions of time, as defined in later sections.

222 **Sediment sources**

223 As in studies of sediment accumulation in other environmental contexts (e.g. marine
224 basins: Kemp 2012), we partition the total sediment flux in to two sources, 'internal' and
225 'external'. This reflects the sediment internally 'recycled' between adjacent landscape
226 surfaces (due to contemporaneous and spatially heterogeneous erosional and

depositional processes on dunes and across interdunes) and that transported from afar, for example from coastal zones exposed through sea level fall (e.g. Preusser, 2009) and from dried or seasonally dry river channels (e.g. Cohen *et al.*, 2010). Separating sediment sources in this way provides the possibility of weighting the relative contributions from each and allowing these to vary through time.

Internal source and variability

If internal recycling were the sole sediment source for the modelled system, and if all sediment were recycled, then on average we would expect no change in surface height, because (on average) the amount lost from the surface would be equal to the amount deposited on the surface. That is, if sand is eroded from one location it must be deposited at another, hence total mass is conserved (which could be expressed equivalently as a constant average surface height). This condition cannot be strictly true for real landscapes as there will always be losses from edges, but it may be a good approximation (although this is not a model requirement). In the present model Q_m can be interpreted as the potential 'internal' sediment flux and the parameter ε is introduced to control the net effect of this flux on the surface – i.e. whether there is net erosion or net deposition. Setting $\varepsilon=0$ simulates equal erosion and deposition throughout the modelled year (any eroded material is re-deposited). In the extreme case of full deposition (any sediment transported to the surface is deposited) ($\varepsilon=1$), then the surface can potentially accumulate continuously (when $u_{eff} > v_T$). The converse situation of continuous erosion arises if $\varepsilon=-1$.

In reality, sampling down into desert sediments in order to extract sediment for analysis and dating represents a point in the landscape. At this spatial scale, the balance of erosion/deposition clearly does not remain fixed over relevant timescales - desert surfaces are heterogeneous and dynamic. For example, increases in windspeed over

an entire landscape are likely to cause erosion/deposition of various degrees in different locations, depending on local geomorphology, slope angle, and so on. Explicitly accounting for these changes would require simulation of the entire landscape surface, but even if this were achieved it is not realistic to expect faithful simulations of specific cases in space and time (rather, the statistical nature of the resultant changes in topography would be modelled). In the current model, we introduce a degree of randomness to implicitly account for spatial variability in local erosional/depositional conditions, and therefore variations through time at fixed locations. Figure 5(i) shows a simplified representation of a transverse dune migrating downwind, and an indication at three distinct times of the positive (accumulation)/negative(erosion) mass balance at various locations (*a* to *f*) at each of these times. We argue that on real desert surfaces, over long timescales, the effect of different dune features, of different sizes, moving at different rates and in varying directions over each location, is likely to yield time series of net-mass-balance which can be well represented as a random process (*c.f.* Kemp, 2012 and in this case, random values of ε). Sadler (1981) and Anders *et al.* (1987) noted, in the marine context of their sedimentation models, that processes of deposition and erosion are not purely random. The same issue applies in our dunefield context: allowing ε to vary randomly each year would ignore the 'geomorphic memory' that exists in desert landscapes, such that locations which experience net deposition one year are more likely to experience deposition over some number of following years (as in the case of accumulating dune-forms, for example). To account for this we produce a vector $\varepsilon = \{\varepsilon_1, \varepsilon_2 \dots \varepsilon_n\}$ which consists of randomly selected values ε_i ($\varepsilon_i \sim N(\mu_\varepsilon, \sigma_\varepsilon)$), which determines the degree of erosion/deposition in subsequent episodes, and another, $\mathbf{T} = \{T_1, T_2 \dots T_n\}$, which determines the number of years (T_i) each such episode persists, $T_i \sim U(1, T_{max})$. An example is shown in Figure 5 (ii), using $\mu_\varepsilon = 0, \sigma_\varepsilon = 0.5, T_{max} = 50$ (values used in all

subsequent simulations). A consequence of setting $\mu_\varepsilon = 0$ is that change in land surface height will average to zero over long time periods, but over shorter timescales (when $\sigma_\varepsilon > 0$) fragments of the sedimentary record will survive for finite periods, reflecting known geomorphological processes in desert landscapes.

External source, s

Key factors controlling the magnitude of input from an external source include the size, erodability and proximity of the sediment source, plus the environmental conditions responsible for erosion/transport/deposition of material. We define s ($s \geq 0$) as a scaling between the effective size of the external source and target (sediment receiving) regions. The value of s may change over time, reflecting changes in the erodability/availability of source sediments (as, for example, bodies of sediment are exposed/inundated due to changes in sea level or groundwater). We chose not to apply the precipitation-dependent scaling (k_m) to the transport rate (Q) of the external source as in reality an external source is not necessarily geographically close to the sampling location and is likely to have a markedly different environmental history. For example, sediment supply to parts of the Strzelecki dunefield in central southern Australia are related to river flow regimes which are linked to distant, northerly, tropical monsoon dynamics (Cohen *et al.*, 2010). Further, the parameterization of moisture effects through k_m cannot necessarily be assumed to be relevant to the source area as the exposure of available sediments may be a relatively short-lived event, and insufficient to allow the kind of quasi-equilibrium landscape states used to justify the k_m parameterization. Instead, we use the dry flux rate (Q) to calculate the potential flux and modulate the magnitude of the external contribution directly, using s . At times when net deposition occurs at the modelled surface (when $\varepsilon > 0$), a contribution from the external source is included; the presence/absence of an external source has no effect on the

modelled surface when it is being eroded, however, and therefore s is set to zero when $\varepsilon \leq 0$.

Mass flux and changes in surface height

The change in sediment mass through time at the simulated surface, as outlined in previous sections, is written as

$$\frac{dm}{dt} = \begin{cases} (sQ + Q_m)\varepsilon, & \varepsilon > 0 \\ Q_m\varepsilon, & \varepsilon \leq 0 \end{cases} \quad (\text{Eq. 6a,b})$$

where Q and Q_m are as described in previous sections. The mass flux can be equated to a volume of sand (and therefore depth, over a 1 m^2 area) by dividing by the appropriate density, here k_q (which we take as $2,000 \text{ kg/m}^3$, for packed quartz-rich desert sand). The evolution of surface height (z) as a function of time (t) is therefore defined as the time integral

$$z(t) = \begin{cases} \int_0^t k_q(sQ + Q_m)\varepsilon dt, & \varepsilon > 0 \\ \int_0^t k_q Q_m \varepsilon dt, & \varepsilon \leq 0 \end{cases} \quad (\text{Eq. 7a,b})$$

with initial condition $z=z_0$. Integration was performed numerically in MatLab® (version R2010a; code written by RB) using the *ode23* solver (an explicit one-step Runge-Kutta algorithm), with evaluations returned for each model year.

Figure 6 provides a simple example, illustrating some of the key elements of model behaviour. Here, precipitation is constant at 300 mm/yr ($p_0 < 300 < p_1$) and u_{eff} is constant at 7 m/s for $0\text{--}500 \text{ yr}$ and 8 m/s thereafter ($u_{\text{eff}} > v_T$) (Figure 6(i)). Figure 6(ii) shows the change in surface height through time for two extreme cases: $\varepsilon=1$ (maximum possible deposition) and $\varepsilon=-1$ (maximum possible erosion) ($z_0=0$); also shown is the accumulation rate for the case where $\varepsilon=1$. The calculation of surface height through time provides data to calculate the resultant age versus depth profile at the end of the model run ($\varepsilon=1$). In this simple scenario (Figure 6(iii)) the change in deposition rate due

to change in effective windspeed at year 500 is visible as the point of inflection at ca.10.5 m depth.

In the following section, further simulations are described which show other aspects of model behaviour under idealized forcing conditions. In these, randomness is included on windspeed, precipitation and ϵ and there is a specific focus on the resultant age distribution of the sediments preserved.

Model behaviour

Experiment 1: intrinsic variability

Because ϵ is different for each model run, results of simulations with identical underlying mean forcings (μ_{ueff} and μ_p) produce different results; additional variability is due to the random sampling through time for these variables, controlled by σ_{ueff} and σ_p). This intrinsic variability in model results reflects the spatial variability observed in desert processes, as described above. In the context of interpreting dune stratigraphy, a useful exercise is to examine what might be termed a 'null' model run, where mean forcings remain constant and variability arises purely from the randomness in ϵ , u_{eff} and p . As an example, Figure 7(i) shows results from a 1 ka model run where $\mu_{ueff}=7$, $\sigma_{ueff}=1$, $\mu_p=300$, $\sigma_p=100$. The simulated surface height shows both increases (accumulation) and decreases (erosion), and in the results shown there is a net increase in surface height of ~2 m. Nevertheless, much of the sediment originally deposited was subsequently eroded and only fragments (ca.50%) of the full record remain, as indicated by the bold symbols overlaid in Figure 7(i) (an example of information loss due to erosion). From these data, accumulation rates for the surviving sediment can be calculated as $\Delta z/\Delta t$ and are shown in Figure 7(ii) (Δz is the difference in surface height from year to year and Δt is the time difference between each point; note that because $\Delta t=1$, the rates are also equal to the total accumulation). Using the data from only the preserved

1
2
3
4 354 sediments, the resultant age/depth stratigraphy can be calculated, and is shown in
5
6 355 Fig.7(iii), where depth is that below the final surface height. Subsequent model runs
7
8 356 produce different simulated stratigraphic records – a situation equivalent to coring more
9
10 357 than once within the area affected by the same past forcings. A sense of what might be
11
12 358 expected *on average*, and over longer timescales, emerges from combining many such
13
14 359 records by summing the resultant accumulation rates for each year of the simulation
15
16 360 (i.e. summing the data equivalent to those shown in Figure 7(ii) from each repeat
17
18 361 simulation). Figure 8 shows such results for 500 repeats runs of a 10 ka simulation, run
19
20 362 under the same (stable) forcing conditions as those used for Figure 7. A strong
21
22 363 preservation bias is seen toward younger sediments, with increased accumulation at
23
24 364 later simulation times. These results are equivalent to a relative probability distribution,
25
26 365 that is, the probability of finding sediments of a given age in a single core: there is a
27
28 366 higher probability of sampling younger rather than older sediments. For deposits older
29
30 367 than ~400 years, the relationship of accumulation magnitudes versus time is well-
31
32 368 described by a power law, decaying approximately in proportion to $1/\sqrt{age}$, as shown
33
34 369 in the inset to Figure 8 (see caption for details). The implication is that if conditions
35
36 370 allow relatively stable average levels of sediment transport over an extended period,
37
38 371 compilations of stratigraphic data are expected to show a similar pattern, with a greater
39
40 372 frequency of younger samples. This observation is examined in the discussion section.
41
42 373 A further series of model experiments are described below. These are not intended as
43
44 374 realistic representations of natural forcings, but rather are simplified scenarios, borne of
45
46 375 the types of climatic forcing changes that may have affected dunefields during the
47
48 376 Quaternary, and designed to demonstrate model behaviour.
49
50 377
51
52
53
54
55
56
57
58
59 378 *Experiment 2: Linear trends in forcing*
60

Figure 9(i) and (ii) shows results from a set of simulations ($n=1,000$) where precipitation changes linearly over 1,000 years from between 500 and 0 mm/yr (decreasing in Case A and increasing in Case B); mean effective windspeed (μ_{ueff}) is constant at 7 m/s throughout the simulation. As in subsequent figures, the degree of variability (noise) in windspeed and precipitation is indicated over the first 100 s (Figure 9(i)), but for clarity only $\mu_{ueff}(t)$ and $\mu_p(t)$ are shown for $t>100$ s. In case A, sediment accumulation rates increase as time progresses as μ_p approaches p_0 (Figure 4(i)). The resultant accumulation potential is a combination of both this effect and the preservation bias towards younger deposits (the effect seen in Figure 8 is amplified as the sediment flux increases over time). Figure 9(ii) also shows the case of a linear increase in precipitation (labelled B). As expected, the total accumulation reduces, as dictated by Eq.5 (Figure 4), but remains above zero in this case due to the variability in p ($\sigma_p > 0$) producing some values of p less than p_1 (controlled by the value of σ_p as μ_p increases above p_1).

Experiment 3: peaks in forcing

Figures 9 (iii) and (iv) show results from three sets of model runs (labelled C,D,E) where forcings vary through time as Gaussian peaks, representing idealised wet and dry periods, with and without correlated increases in windspeed ($N=1,000$ in each case). The various combinations of windspeed and precipitation forcing are shown in Figure 9(iii). For case C (*dry period*), effective windspeed remains constant at 7 m/s and precipitation dips from 600 to 0 mm/yr (for clarity, noise in windspeed and precipitation is not indicated on figure, but is nonetheless included in the simulations, with $\sigma_{ueff} = 1$ and $\sigma_p = 100$, as in case A and B shown in Figure 9(i)). High levels of precipitation halt sediment mobility prior to $t \approx 300$ and following $t \approx 750$. There is deposition during the dry period, and a preservation bias is seen in the slight asymmetry of the sediment

response (vertical dashed lines are included in the figure as visual aids). The converse is true of case D, where dry conditions are interrupted by a *wet period*, in which precipitation is sufficiently high to fully inhibit sediment mobility and the accumulation rate drops to zero. A strong preservation bias is seen in the increased accumulation rates of sediments from $t=700$ onwards. In case E, an identical dry spell correlates with an increase in windspeed. Because u_{eff} is below the threshold velocity ($v_T = 6.4 \text{ m/s}$ for $200 \mu\text{m}$ grains) until near the peak in windspeed, and because the peak windspeed is greater than the constant level of cases C and D, the sediment response is more exaggerated, both in its abruptness and magnitude (note the scaling in Figure 9(iv), data E).

Experiment 4: Response in the presence of significant external input

In the model experiments described in previous sections, parameter s was held constant at zero. This parameter provides a scaling to the potential dry flux (Q), which is included during depositional phases (when $\varepsilon > 0$) and can be varied through the experiment to simulate changes in the effective magnitude of an external source. Figure 10(i) and (ii) show data from experiments with both mean windspeed and precipitation held constant ($\mu_{u_{eff}}=7$, $\sigma_{u_{eff}}=1$, $\mu_p=300$, $\sigma_p=100$, as in Figure 7), with the addition of Gaussian-shaped pulses of external sediment centred on $t=500 \text{ yr}$, reaching maximum values of 0.1, 0.5 and 1.0. In each case, 1,000 repeat simulations were run and the results shown in Figure 10(ii) represent the mean accumulation rate over all 1,000 runs. The continuum of accumulation due to preservation bias is observed in the rising limb over the range $800 < t < 1000$, and the peak due to external sediment contribution is seen as an addition to this. These results suggest a contribution of $>0.1Q$ is required for an external contribution to be observable beyond the background continuum (depending on the age of the external sediment influx, and therefore the magnitude of the

continuum, smaller external contributions may be visible in older records but the limit is not likely to be substantially less than $s=0.1$; see also caption to Figure 10(i)). Figures 10(iii,iv) show results for a case where peaks/troughs in wind and moisture forcings are not coincident in time (in contrast to previous simulations). The justification for modelling this (non-coincident) forcing scenario is provided in some recent literature assessments of dune behaviour through time. Different periods of Late Quaternary and Holocene dune accumulation have been attributed respectively to increased windiness or to increased dryness but not the two simultaneously (Chase, 2009). For example, for the west coast dunefields of southern Africa, Chase and Thomas (2006) propose increased windiness as the prime driver of dune construction in four phases within the period 73-16 ka, whilst dune activation at 8-4 ka, the Holocene altithermal, is attributed to a reduction in moisture caused by higher temperatures and reduced rainfall, but no wind energy changes. In parts of Australia, Hesse et al. (2003) have also suggested complex relationships between wind and moisture variables influencing dune activity. In the present modelling case, a peak in external sediment follows non-coincident fluctuations in precipitation and windspeed, resulting in the accumulation data shown in Figure 10(iv). The lower timeseries (labelled I) is the case where no external sediment input is included ($s=0$), and line 'J' includes the forcing shown in Figure 10 (iii). The enhanced accumulation peaking at $t \approx 600$ yr coincides with the peak in s .

Geomorphological settings with positive net mass balance

In real desert systems it may be the case for some geomorphic settings that while both erosion and deposition take place over relatively short timescales, accumulation is more likely than erosion for extended periods. Subsiding basins, or extending linear dunes may fall into this category. This situation can be simulated in the present case by setting $\mu_e > 0$, so that on average the probability of deposition is greater than that of erosion.

1
2
3
4
5
6
7
8
9
10
11
12
13
14
15
16
17
18
19
20
21
22
23
24
25
26
27
28
29
30
31
32
33
34
35
36
37
38
39
40
41
42
43
44
45
46
47
48
49
50
51
52
53
54
55
56
57
58
59
60

For brevity, results of such simulations are not shown but similar patterns to simulations where $\mu_{\varepsilon} = 0$ are observed, with an enhanced accumulation, in proportion to μ_{ε} (both a larger continuum component and enhanced responses to relevant forcings).

Summary of findings from simulated forcings

As dictated by Eq.(7) potential deposition is determined by both windspeed and precipitation. Windspeed controls the magnitude of the potential sand flux and precipitation determines the proportion of this potential that is realised (and therefore the potential magnitude of erosion/deposition). Changes in external sediment supply affect deposition and the resultant sediment preservation in proportion to the magnitude and duration of the external input. However, as this contribution is made only when wind and precipitation parameters allow transport/deposition to occur, external sources act to amplify and enhance local depositional processes. Drier periods are those with the greatest potential for erosion and deposition and as a consequence drier periods dominate the preserved records in the simulations. A net preservation bias towards the end of active (sediment transporting) periods is observed, which extends for several thousand years, decaying approximately in proportion to $1/\sqrt{age}$, meaning that a greater amount of younger sediment is expected to be preserved, leading to a larger number of younger dates, as discussed in the following section. Importantly, different model runs, with the same underlying forcing conditions (these simulations being equivalent to different locations within the same region) yield preserved records which differ markedly, the implications of which for empirical studies are discussed below.

Simulated dating of simulated stratigraphies

To simulate the dating of preserved sediments, the sampling process must be mimicked. To achieve this the simulated sediment age at prescribed depths of each

simulated stratigraphy is recorded. Sampling resolutions of 1 m and 0.5 m were used, and virtual sampling was continued for each simulated stratigraphy until the base of the material relating to the simulation period was reached. This mimics the physical sampling of desert dunes described, for example, in Telfer and Thomas (2007), where ages are obtained on recovered dune samples using OSL dating (as discussed in the introduction). As with all real dating methods, the dates are subject to both random and systematic errors. In the present simulated case we ignore any potential systematic errors (i.e. we assume that the dating 'works'), but do include the effect of random errors, which in real dating applications are due to the measurement process and parameter uncertainties propagated through the age calculations. To simulate the scattering effect of random errors, a random variate of each date was created. The magnitude of the relative uncertainty is not constant for all dates in empirical studies and here is chosen randomly from a Gaussian distribution of possible uncertainties. For an initial simulated sediment age α , the resultant date a is calculated as

$$a = \alpha + abc \quad (\text{Eq.8})$$

where b is a random value selected from a standard Normal distribution ($b \sim N(0,1)$) and c is the relative uncertainty of the date ($c \sim N(0.08,0.02)$), but truncating this distribution so that no value of c is below 0.04. An average relative uncertainty of 8% reflects typical dating precision (of individual dates) in desert environments using current methods; the lower limit of 4% reflects the likely fundamental limit to precision for optical dating, and 12% is a fair estimate of the typical worst-case (larger uncertainties are common in older methods, such as the application of TL dating and multiple-aliquot OSL methods).

As an example, to demonstrate the variability in the simulated stratigraphies, Experiment 5 is a set of model runs, each 10,000 years duration, with a single 'wet event' on a background of an otherwise dry conditions (as indicated in the lower right

1
2
3
4 509 panel of Figure 11; see caption for further details). Figure 11 shows six simulated
5
6 510 stratigraphies. The vertical lines delimit relevant parts of the wet event (where mean
7
8 511 precipitation levels cross values p_0 and p_1 ; see caption to Figure 11). The paucity of
9
10 512 dates where mean precipitation is above p_1 is evident, but without the benefit of prior
11
12 513 information on the wet period, identifying it from the dates alone would be less
13
14 514 straightforward, particularly given the level of scatter. For example, contrast the well-
15
16 515 separated groupings of dates in Figure 11(iv) to the seemingly constant accumulation
17
18 516 rates through this period seen in parts (ii) and (iii). These results, together with many
19
20 517 empirical results, lead naturally to questions of resolution, that is, what events can
21
22 518 potentially be resolved with confidence from stratigraphic data and what analytical
23
24 519 methods, beyond 'eye-balling' the data, might be employed to aid interpretation. To
25
26 520 provide relevant theoretical data with which to address these questions, Experiment 6
27
28 521 (as described below) was run, and analysed using methods described in the following
29
30 522 section. A discussion of both theoretical and practical limitations on the interpretation of
31
32 523 stratigraphic data are given in the main discussion section.
33
34
35
36
37
38
39
40

41 524
42
43 525 *Methods of analysis*
44
45 526 Perhaps the most basic analysis of dune dating results is of frequency; here, this is
46
47 527 represented by the number of dates observed (over all cores) within specified time
48
49 528 windows. The logic is that there should be more material deposited in more active
50
51 529 (drier, windier) periods compared to less active (wetter, calmer) periods, and therefore,
52
53 530 all other factors being equal, more dates are expected to be derived from more active
54
55 531 periods. A second measure of activity, accumulation rate, follows a similar logic: the
56
57 532 deposition rate of sediment in the preserved record should on average correlate with
58
59 533 the level of geomorphological activity, and this should be reflected in the effective
60
534 accumulation rate. Here, this was calculated for samples of each core as

$$r_z = |\Delta z_z / \Delta a_z| \quad (\text{Eq.9})$$

where Δz_z is the difference in depth between the sample at depth z and the sample below (z_{\downarrow}), $\Delta z_z = z - z_{\downarrow}$; equivalently, Δa_z is the difference in age, $\Delta a_z = a_z - a_{z\downarrow}$. However, because each date is not a single unique value, but rather a distribution, reflecting the possible dates that could have been obtained from repeated measurements (i.e. random uncertainties), these distributions should be included in calculations of frequency and accumulation rates. To achieve this the randomization process (Eq.8) is repeated N times for each date (sampled depth remains constant), and accumulation rate and frequency calculations are performed on these sets of data, producing distributions of each metric (within successive time windows – described below). N is chosen to be sufficiently large that the mean (μ_σ) and standard deviation (σ_α) for each set were stabilized ($N=10,000$).

As demonstrated in the present modelling context in Figure 11, and empirically, for example by Stone and Thomas (2008) and Atkinson *et al.* (2012), dates from individual cores provide only partial information on past changes in underlying forcings, presumably because of the spatial variations in erosion/deposition rates discussed in previous sections (parameterized by ε in the present model), which typically lead to non-linear relationship between time and sediment thickness (e.g. Kemp, 2012). Amalgamating many such results to reduce the impact of local variation is therefore essential. This is in effect the approach taken in some recent empirical studies where multiple cores are used and ages are pooled in the analysis (e.g. Telfer and Thomas, 2007, Stone and Thomas, 2008). Here, we calculate the frequency of date occurrence, in 100 year bins, for all 10,000 variants (described above) of each date and over each of the simulated cores. Similarly, for each sampled depth, the average and standard deviation of accumulation rates of the variants that fall within each 100 year bin are calculated. The mean and standard deviation of both the date frequency and

1
2
3
4 561 accumulation rates therefore change through stratigraphic time, reflecting the depths
5
6 562 and ages of the samples. Changes in the standard deviation of the accumulation rates
7
8 563 through time ($s_{rz(t)}$) can be used as a proxy for aeolian activity (discussed below) and
9
10 564 this is based on the following logic: two overlapping dates, separated by a given depth,
11
12 565 will produce a relatively wide range of possible accumulation rates using the random
13
14 566 sampling approach described above (reflecting the relatively high accumulation rate);
15
16 567 conversely, if at these same depths, the sample ages were significantly separated, the
17
18 568 range of possible accumulation rates would be considerably lower (becoming lower for
19
20 569 greater age separation), reflecting either a low accumulation rate or, more likely, a
21
22 570 hiatus. In cases where the sampling depths are evenly-spaced, as in the present
23
24 571 simulation data, s_{rz} provides a robust proxy for accumulation rate, and hence past
25
26 572 aeolian activity, when data from multiple cores are amalgamated. That is, erosional
27
28 573 gaps in individual records covering periods of high activity will be expected to be filled
29
30 574 by the addition of further records, but gaps (episodes of low activity) will persist.
31
32 575 Because standard deviation does not change systematically with sample size (but
33
34 576 instead approaches the true value as sample size increases), over-representation of
35
36 577 some (typically more recent) parts of the record due to sampling (frequency) bias does
37
38 578 not affect s_{rz} (which remains a problem in the various frequency and pdf-related
39
40 579 methods used in some empirical studies to display data and aid interpretation). We term
41
42 580 this method of analysis *accumulation-rate-variability* (ARV). Data produced using the
43
44 581 ARV method in this current form are affected both by inter-sample differences in
45
46 582 sampling interval and dating precision, which effectively add noise to the signal. These
47
48 583 influences are insignificant in the case of the present model data, but may be more
49
50 584 important in empirically-measured datasets. The sensitivity of results, and modifications
51
52 585 to the method to correct for introduced bias are explained in a forthcoming publication
53
54
55
56
57
58
59
60 586 (Bailey *et al.*, *in prep.*).

587

588 *Time resolution*

589 Because all dates have uncertainties, dated events separated by relatively small time
590 intervals will not be separable chronologically; that is, error bars will overlap and no
591 difference in age will be resolvable. This has relevance to the present work as this
592 effect provides an increasingly wide smoothing window which filters out higher
593 frequency variability as sample age increases. This is explored in Figure 12(i), which
594 shows results from a series of numerical calculations which simulate the dating of pairs
595 of 'true dates' to assess the probability of successfully identifying age differences. The
596 true dates (t_1 and t_2) provide the means of Gaussian distributions (with standard
597 deviations equal to 8% of the true age) from which sample dates were drawn
598 (simulating the random scatter induced by the dating process). Each sample date is
599 then assigned an uncertainty (equal to the relative standard deviation responsible for
600 inducing scatter) which defines the dating error bars (i.e. it is assumed that the random
601 error component of the dating uncertainty is estimated accurately). The procedure was
602 repeated 10^6 times for each pair, over 1 ka increments for both true ages (t_1 , t_2) ranging
603 from 1 to 100 ka. The proportion of dates that was chronologically distinguishable at 1
604 sigma (non-overlapping error bars) was recorded for each pair of true ages. These data
605 are summarised in Figure 12(i) by 90% and 50% contours (of the overlap percentages
606 in t_1, t_2 parameter space); above the 90% contour, overlap between age estimates
607 happened in less than 10% of cases and therefore a 90% success is expected in
608 distinguishing between the two co-ordinate dates (t_1 on the horizontal axis and t_2 on the
609 vertical axis of Figure 12(i)). The 90% contour can be used to look up the minimum time
610 separation between events necessary in order that the events be resolvable
611 chronologically (with 90% confidence, reflecting what we judge to be an appropriate
612 balance between Type I and Type II errors in this context). An example using 70 ka as

the reference age is demonstrated in Figure 12(i). We can write the relationship between t_1 and t_2 as $t_2 = \beta t_1$ (for data in Figure 12(i), $\beta = 1.3581$ for 90% and $\beta = 1.1739$ for the 50% contour). β must depend on dating precision and by repeating the calculations described above for dating uncertainties spanning 4-14%, the relation $\beta = \exp(3.84\sigma)$ was obtained (for 90% 'success'), where σ is the relative dating uncertainty. Using these relationships, it is useful to estimate the age at which a given time gap in the record becomes unresolvable (at the given level of confidence), which provides a quantification of the degree of 'smoothing' of the record. The age above which a time gap between depositional events (denoted g , in units of ka) becomes unresolvable is t_2 , when $g = t_2 - t_1$, and to avoid confusion we refer to this date as t^* ($t^* = t_1 + g$). Because $t_2 = t_1 \cdot \exp(3.84\sigma)$ we can write $g = t_1 \cdot \exp(3.84\sigma) - t_1$ and solving for t_1 yields $t_1 = g / ((\exp(3.84\sigma) - 1))$, hence $t^* = g / ((\exp(3.84\sigma) - 1)) + g$. This represents the date beyond which gaps of size g are likely to be 'lost from view' (and therefore indistinguishable from continuous deposition) in individual cores. This relationship is plotted, for different levels of dating precision, in the main part of Figure 12(ii). Above this, a representation is given of the spacing between depositional events necessary for each to be resolved, and is described more fully in the figure caption. Further discussion of the implications for the filtering out of higher frequency variability in the stratigraphic record can be found in the Discussion section.

Experiment 6: Simulated dating of multiple wet and dry events

Experiment 6 consists of two main sets of experiments (a & b), simulating multiple wetter/drier phases, of different durations. Experiment 6a simulates 'dry' events on a background of otherwise 'wet' conditions; 7b simulates 'wet' events on a background of otherwise 'dry' conditions. Each simulation lasts 10,000 years, with mean effective windspeed constant throughout (details in caption to Figure 13). Mean annual

precipitation is 100 mm/yr during 'dry' conditions, and 600 mm/yr during 'wet'. Nine changes from the background condition to wet/dry conditions were simulated, at 1,000 year intervals from $t=500$ to $t=8,500$. Three event durations were used (after which precipitation was returned to the background level): 50, 200, 500 yr. Therefore, for each 10,000 yr simulation, precipitation varies as a 'square-wave', simulating abrupt changes in forcing conditions (rather than the more gradual changes of previous experiments). Each experiment was repeated 50 times, mimicking the collection of multiple cores, and the ('virtual') sampling of each simulated core was undertaken as described above, at 0.5 m intervals. The number 50 was chosen to reflect the likely practical limit to the number of cores which could be taken in any given region, although in principal this number could be increased. An additional set of simulations (Experiment 6c) was run, equivalent to Experiment 6a (with event durations of 500 years), but with mean precipitation values of 400 mm/yr ('wet') and 200 mm/yr ('dry') representing less extreme oscillations in conditions. Data from these experiments are presented in Figures 13-15. Figure 13(i) shows data for dry events lasting 200 years and Figure 13(ii) provides data for equivalent wet events; in both cases, data from all 50 cores were used. In each case, four sets of data are shown: 'Age frequency' (top) is the mean (\pm standard deviation) of re-sampled age data (as described above); 'Accumulation rate' shows equivalent (mean \pm standard deviation) data; ARV (the 'Accumulation rate standard deviation', $s_{rz(t)}$, defined above) is shown below this and the precipitation forcing is the bottom plot in both (i) and (ii) (Experiments 6a and 6b). Each data set is vertically scaled and offset, to facilitate visual comparison (the vertical axis is arbitrary). Figure 14 is a series of ranked-age plots, in which dates from an increasing number of cores (parts (i) to (iv)) are plotted in age order, as is common in empirical dating studies. To the right of each part, vertical bars indicate the time period occupied by the dates. In each panel of Figure 15 age frequency (\pm standard deviation) is the upper

1
2
3
4 665 plotted data series (data from Experiment 6a) and Accumulation rate standard deviation
5
6 666 (labelled ARV) are shown below this (for Experiment 6a, labelled [100,600] reflecting
7
8 667 the extremes of mean annual precipitation, and for Experiment 6c, labelled [200,400]),
9
10 668 above an indication of the precipitation forcing. All are plotted on arbitrary vertical axes,
11
12 669 as in Figure 14. *N* values refer here to the cumulative number of virtual cores
13
14 670 (simulation repeats) used to construct the data, as described above: *N*=5 means cores
15
16 671 1-5 were used, *N*=10 means cores 1-10 were used, etc.. Interpretation of data from
17
18 672 Experiment 6 is provided below in the discussion section.
19
20
21
22
23
24

25 674 **Discussion**

26
27 675 The nature of aeolian processes means that both erosional and depositional conditions
28
29 676 operate with a wide range of intensities and over a continuum of durations. Regardless
30
31 677 of environment, no location remains a site of deposition indefinitely; records are
32
33 678 necessarily discontinuous and vary from location to location, on temporal scales from at
34
35 679 least tens of thousands of years down to sub-annually (Kemp, 2012). In OSL-dated
36
37 680 dune sequences we have an additional problem: dating uncertainties limit our ability to
38
39 681 resolve these finer scale breaks in sedimentation, but there is no reason to doubt that
40
41 682 past hiatuses exist at un-observably fine temporal scales (such breaks may or may not
42
43 683 be represented by observable stratigraphic discontinuities, as reported by Leighton *et al.*,
44
45 684 in press). These realities are reflected in the model setup, its results, and also in
46
47 685 empirical evidence (e.g. see discussion in Leighton *et al.*, in press), creating records
48
49 686 which are discontinuous and spatially variable in terms of deposition and preservation.
50
51 687 A change in forcing conditions may or may not be recorded; if it is, it will be recorded
52
53 688 differently at different sites, and subsequent preservation and any sampling for dating
54
55 689 will inherently be heterogeneous. As portrayed in Figure 1, these various processes and
56
57 690 events filter out the information on the primary forcing factors that investigation of
58
59
60

stratigraphic data is designed to obtain. Questions naturally follow, related to topics such as the likelihood of correctly identifying changing conditions in the past, and the kind of events we might expect to be able to practically resolve in the record, versus those we might expect to miss. The discussion that follows is organized under what we consider to be relevant topics.

Wet versus dry

The ability to recognize an 'environmental episode' (a period in which conditions are significantly different from those preceding and/or following it), depends on the nature of the background conditions, the event, its timing and its duration. Sadler (1981) noted the completeness of sedimentary records is likely to decline at finer time scales; we therefore expect a natural bias towards recording more significant (higher magnitude, lengthier) depositional episodes, and overprinted on this is also a preservation bias towards younger sediments. OSL dates from dune sands provide evidence for the timing of past aeolian geomorphological activity (Thomas and Burrough 2012), that is, the re-working and re-deposition of sediment. All else being equal, dry periods are expected to be more active (in both erosion and deposition) than wetter periods, and as such, dated sediment deposition most likely reflects periods of drier/windier conditions, with a preservation bias towards the younger end of such periods, whatever their duration (e.g. Figure 8). In addition to these observations, the present work also gives theoretical evidence for an asymmetry in our ability to use dated sediment records to identify past periods of wetter and drier conditions.

Model results suggest the identification of dry events during otherwise wet periods is considerably more likely than identifying wet events in otherwise dry periods. In wetter periods there is less sediment mobility due to aeolian processes (as described in earlier sections), and large spans of time may be represented by little or no aeolian sediment

1
2
3
4 717 accumulation. An intervening (dry) pulse of aeolian activity will however provide some
5
6 718 locations with a significant body of re-worked/deposited material (possibly the only
7
8 719 depositional event between the dry event and the time of sampling). Under the wetter
9
10 720 conditions that follow, this material is less likely to be eroded by aeolian processes and
11
12 721 subsequent coring is therefore likely to sample it. Conversely, in an extended dry
13
14 722 period, where there is frequent re-working/re-deposition, and where hiatuses in
15
16 723 individual stratigraphies are common, a wetter (less active) environment provides
17
18 724 essentially just another additional time period for which deposition is effectively absent.
19
20 725 Without other direct 'wet episode' proxy records (a common situation in dunefields),
21
22 726 confidently ascribing a stratigraphic gap to wetter (low-activity) conditions requires the
23
24 727 other gaps in the sampled record (due to under-sampling) to be filled by additional
25
26 728 sampling. Identifying 'wet event gaps' is therefore in principal possible, but the number
27
28 729 of dates/cores required may be large, and depends on the magnitude/duration of the
29
30 730 event, the age of the event and the precision of the dating method employed (further
31
32 731 discussion below). Example data in Figure 13 (Experiment 6) show that in both the
33
34 732 frequency and ARV analyses, for wet/dry event forcings of the same magnitude,
35
36 733 duration and spacing, 'dry events' (Figure 13(i)) are considerably better-resolved in the
37
38 734 record than the equivalent 'wet events' (Figure 13(ii)). We note also the encouraging
39
40 735 results from Experiment 6c (Figure 15) which shows the ARV method is capable of
41
42 736 identifying wetter/drier periods when the differences between these periods is
43
44 737 considerably less exaggerated (mean annual precipitation 200-400 mm/yr compared to
45
46 738 100-600 mm/yr), suggesting relatively high sensitivity to precipitation forcing. This
47
48 739 aspect of environmental reconstruction from dune sediments requires further
49
50 740 investigation.
51
52 741
53
54
55
56
57
58
59
60

742 *Temporal resolution and gaps in the record*

1
2
3
4 743 In cases where sedimentary units can be uniquely defined in terms other than their age,
5
6 744 for example using biostratigraphic or morphostratigraphic criteria, the accumulation of
7
8 745 multiple dates from such units may result in relatively high precision age estimates and
9
10 746 relatively highly resolved records (for example, compare 4% and 8% precision in Figure
11
12 747 12(iii)). However, in perhaps the majority of cases, one sand unit (within a particular
13
14 748 region) looks much like another and few reliable environmental proxies, with potential
15
16 749 stratigraphic markers, are preserved. This is a situation widely recognised in southern
17
18 750 Africa (Telfer and Thomas 2007), though in some contexts, such as the Australian
19
20 751 dunefields, widespread recognition of weak palaeosols is claimed (Hesse, 2011). As a
21
22 752 consequence, in many contexts it is not possible to know whether spatially separated
23
24 753 units represent responses to the same or different forcing events, and therefore
25
26 754 individual age estimates cannot be assigned to groups for which pooled statistics can
27
28 755 be applied (i.e. where uncertainties on unit ages can be reduced by repeated
29
30 756 independent measurements, at different sampling locations which do not share site-
31
32 757 specific systematic errors). In such cases, the resolution of the record is set by the
33
34 758 precision of individual dates. As the rapidity of changes in forcing increases, evidence
35
36 759 of geomorphic response to individual events is expected to become harder to
37
38 760 distinguish, and this raises questions regarding the resolution (and hence utility) of the
39
40 761 record. Present model results suggest, perhaps counter to intuition, that events of
41
42 762 almost any duration may leave a stratigraphic record (in the model the shortest time
43
44 763 interval is one year). In real situations, for example, a single sand storm may deposit a
45
46 764 significant amount of sand at some depositional sites. The duration of an event cannot
47
48 765 be resolved to better than the true duration of the event plus some multiple of the
49
50 766 uncertainty (depending on the desired confidence, but ≥ 2), which is proportional to
51
52 767 sample age. This is evident in data (not shown) from Experiment 6, where depositional
53
54 768 events of different durations were simulated. Therefore, whether individual events can
55
56
57
58
59
60

be resolved chronologically (given they have been sampled) depends less on the duration of the event and more on the time gap between depositional events in relation to the dating errors (which depend on age). For a given gap duration (g) we have defined (see above) a critical age limit (t^*) as that beyond which individual depositional events cannot be resolved, and this limit depends sensitively on dating precision. In effect, an apparent continuum of dates may be obtained if depositional events are not sufficiently separated in time (e.g. Figure 14). Individual OSL dates currently have a maximum possible precision (a minimum random uncertainty) of approximately $\pm 4\%$ of the sample age (due to uncertainties in factors such as moisture content, over-burden history, laboratory radiation source calibration and radioisotope half-lives: any claims to greater precision need to be treated with extreme caution). In the present work we have taken $8 \pm 2\%$ as a typical relative error magnitude for dated desert samples (see Figure 12(ii) for implications). If a distribution of gap durations exists, and there is little reason to doubt this, individual events with shorter separation times will be progressively filtered out of the available record as age increases (this is borne out in the model results presented in Figures 13 and 15), potentially leading to a false impression that changes in the more distant past occurred less frequently than in more recent times.

As discussed above, much of our ability to interpret dune sediments rests on the correct treatment of stratigraphic gaps. Genuine gaps in modelled sediment accumulation are due to relatively wetter and/or calmer conditions (e.g. Figure 9(iv)); peaks in activity (either above the level of the continuum or in an otherwise stratigraphically unrepresented time period (e.g. Figure 9(iv))) are due to drier and/or windier conditions. However, how this picture relates to modelled, and by extension real, sample dates is less straightforward. Gaps in individual stratigraphic records must be present if there is indeed a uniform and widespread break in sedimentation (due to regionally wetter conditions, for example), and valuable environmental information is therefore potentially

available. However, as discussed above, two factors complicate this picture: under-sampling of the record and the effect of dating uncertainty (other geomorphological complications are discussed further below). It is not possible to distinguish between sporadic and continuous aeolian activity if the depositional events are closely-spaced in time (within dating uncertainties) and this provides opportunities to overlook 'true gaps' (and therefore changes in past forcing conditions). Conversely, 'false gaps' may be present because of under-sampling. As the number of cores increases, we would expect 'false gaps' to be filled and 'true gaps' to persist. As sampling proceeds, therefore, absence of evidence of deposition is indeed *evidence* (but not proof) of absence of deposition. Nonetheless, a true gap can never be proven from a finite data set, as further cores may provide the previously missing evidence of deposition ('unlucky' sampling can never be ruled out). The assignment of low-aeolian activity 'wet periods' to gaps in the dated dune record is therefore always provisional, in the absence of independent verification, but perhaps defensible where such gaps are shown to be persistent across multiple independent records.

Analysis and the number of dates

As the number of cores obtained increases, and additional data become available, changes in the distribution of dates may lead to progressive (and partly predictable) changes in interpretation. With very few cores the record may appear to show discrete periods of accumulation; as more cores/samples are added, the apparent periods of activity change, and as further data are added, 'gaps' are likely to be filled-in, possibly giving the appearance of a continuum of activity (see for example figures in Telfer and Thomas 2007). The ranked age plots in Figure 14 also demonstrate this progression, even though the underlying precipitation forcing is a square-wave (Figure 14(i)). Attempts to date and interpret dune records are arguably currently stalled in this second

stage (see discussions in Stone and Thomas, 2008). Plotting the ages directly (either as amalgamated age/depth plots or as frequency data) is highly susceptible to sampling-frequency bias and cannot be guaranteed to provide good information on periods of past dune activity (see for example, Thomas and Burrough 2012; Thomas 2013). However, using the new methods described in earlier sections (notably *accumulation-rate-variability*, ARV), periods of higher/lower activity are resolved with greater clarity as the number of cores increases, in contrast to ranked age plots (compare the same age data used to construct Figures 14 and 15). Our conclusion is that information on levels of past activity is encoded more effectively in the accumulation rate data (for which ARV is a proxy) than in the dates themselves (see also Leighton *et al.* (submitted) for additional discussion). The present results do to a limited extent also support analysis of date frequency (as implemented in previous sections, with multiple re-sampling). Whilst requiring relatively large amounts of data (compared to the ARV method), date frequency can provide a useful metric of activity, in cases where the sampling depth resolution is constant between cores, locations are chosen independently, and the coring extends to the base of the record in each case (i.e. ages older than the period of interest are obtained from the base of each core, in order that over-sampling of younger material is minimized).

The question of how many cores/dates are needed before confident interpretations can be made is not easily answered, as it depends on the age, duration, type and separation of events. A useful empirical strategy may be to continue sampling/dating until the results (and therefore the interpretations) remain stable in the face of new data. Figure 15 suggests that for the 'dry events' simulated, 10-20 cores may be sufficient to identify those changes in activity which are indeed possible to resolve (i.e. are separated by adequate time intervals according to calculations of t^*) if the ARV method is employed. The considerable uncertainty in calculated age frequency data (see

caption to Figure 15) would preclude confident identification of peaks in activity until N was large, whereas ARV remains relatively consistent with $N \geq 5$. However, under-sampling of the record affects calculations of ARV more than age-frequency because ARV relies on pairs of dates; if the total core depth covering the period of interest is less than twice the sampling interval (which may be the case following prolonged periods of inactivity with short periods of potential deposition), ARV cannot be calculated. Hence, the 'stable interpretation' described above is, on average, more likely to be achieved using higher resolution sampling. While identifying well-separated (even relatively short) dry events (Figure 13(i)) seems well within the grasp of the methods described, separating more closely-timed 'wet events' from a background of near continuous aeolian activity (e.g. Figure 13(ii)) is considerably more difficult, requiring greater amounts of age/depth data. Higher resolution sampling (here, 0.5 m compared to 1 m) again bestows an advantage by increasing the likelihood of sampling shorter duration events in individual cores, but this advantage decreases as the number of cores increases (shorter depositional events produce shallower stratigraphic units and these are less likely to be missed with more cores at higher sampling resolution).

Modelling of the filtering problem

Figure 1 identifies various types of processes capable of removing and modifying information on past conditions from the stratigraphic record and the effects of each of these processes are included in the present model. For example, the *Primary geomorphic response* (column (2) in Figure 1) is controlled by Eq.5, which is non-linear, and for which there is a response only when windspeed and precipitation are above/below relevant thresholds (see Figure 4(ii)); preservation/erosion of younger deposits (column (3) in Figure 1) is determined by the time-dependent forcing conditions, and for individual 'cores' (model runs) can result in 0-100% removal of the

1
2
3
4 873 previously deposited sediment (and therefore the information on past conditions); the
5
6 874 virtual sampling described mirrors the aliasing effect of field sampling (column 4), and
7
8 875 results in only a small fraction of the available sediment being dated; the dating process
9
10 876 further modifies (smooths) the age/depth profiles through the effect of random
11
12 877 uncertainties (column 5). However, rather than despairing of our chances of gleaning
13
14 878 anything useful from dune records, we are encouraged by the potential of the ARV
15
16 879 method (and others based on accumulation rate data, e.g. Leighton *et al.*, submitted).
17
18 880 Further, we can only hope to make appropriate use of the information we have if these
19
20 881 complicating factors are acknowledged. We note that while the details may be different,
21
22 882 the filtering effect we describe (Figure 1) is present in all environmental proxy/dating
23
24 883 data, and is certainly not a problem only for dune records.
25
26
27
28
29
30
31

32 885 *Comparison to a real-world case*

33
34 886 The southern Kalahari (southern Botswana, Northern Cape Province, South Africa, and
35
36 887 southwestern Namibia) has extensive linear dunes that are well-studied
37
38 888 palaeoenvironmentally (e.g. Stone and Thomas, 2008; Telfer, 2011) and in terms of
39
40 889 contemporary sand transport processes and dynamics (e.g. Wiggs *et al.*, 1995; Bullard
41
42 890 *et al.*, 1996). Currently the dunefield receives low and annually variable precipitation
43
44 891 (mean <150-200 mm/yr), and represents the dry end of a gradient towards wetter
45
46 892 conditions (ca.800-1000 mm/yr) in the northeastern Kalahari, in western Zambia
47
48 893 (Thomas and Shaw, 1991), where relict linear sand dunes also exist (O'Connor and
49
50 894 Thomas, 1999). Following the logic of earlier arguments, and if current conditions have
51
52 895 been the norm for many thousands of years, the likelihood of accurately identifying
53
54 896 periods of wetter conditions in the southern Kalahari is expected to be low (perhaps
55
56 897 sharing some similarities to the simulated case shown Figure 13(ii)). A continuum of
57
58 898 ranked sediment dates akin to Figure 14(iv) would in that case be expected, and this is
59
60

indeed what is found (Thomas, 2013). Conversely, the visibility of drier periods in generally wetter areas, such as western Zambia, is expected to be considerably higher (more like the model data shown in Figure 13(i)). The dated record may currently suggest that punctuated dune sand deposition and preservation has occurred (O'Connor and Thomas, 1999), although a cautionary note must be added given that the dunes of western Zambia have not been sampled/dated with the same intensity as has the southern Kalahari. Additionally, there are non-aeolian processes which may play important (and complicating) roles under wetter conditions, that affect dune sediments. These are not included in the present model, but may affect dated records from the northern Kalahari. These include, for example, localized removal of sediment by fluvial processes, and the reduction of dunes topography by slope wash, which naturally redistributes the upper (younger) parts of sedimentary records to interdune areas as linear dune forms decay (first discussed in Flint and Bond (1968) and recently reiterated by MacFarlane *et al.*, 2005). For these and other reasons, uncertainties will always remain with respect to achieving full interpretations of accumulated dune records, just as they remain, but are often overlooked, with regard to other proxy records of palaeoenvironmental and palaeoclimatic change.

Conclusions

The completeness of stratigraphic records is a significant concern in sedimentology, (Sadler, 1981; Tipper, 1983; Kemp, 2012) and a notable one in aeolian research where dated dune sediments are a critical source of palaeoenvironmental information. This study has provided a simulation of some of the complexities of aeolian records, their relationship to primary forcing, and the difficulties inherent in interpreting the dated records. We draw the following conclusions:

- 1
2
3
4 924 • Because the intensity of erosion/deposition is controlled predominantly by
5
6 925 windspeed, precipitation and external sediment supply, greater levels of past
7
8 926 sediment accumulation relate to more active sedimentary environments and can
9
10 927 therefore be linked to conditions which promote sediment mobility - lower
11
12 928 precipitation levels and greater windspeeds
13
14
15 929 • Over long timescales, a switching between erosion and deposition is expected at
16
17 930 each location, and this can be treated as a random process. Consequently,
18
19 931 discontinuous and highly variable stratigraphic sequences are expected in relatively
20
21 932 close spatial proximity. Multiple dated cores are needed in order to avoid under-
22
23 933 sampling the regional record.
24
25
26
27 934 • A preservation bias means that deposited material is marginally more likely to come
28
29 935 from the end of dry and/or windy periods. Over extended active periods (with
30
31 936 constant average forcings), amalgamated results are expected to show a continuum
32
33 937 of accumulation (and therefore sediment dates), with stronger preservation of
34
35 938 younger material, decaying approximately in proportion to $1/\sqrt{age}$.
36
37
38 939 • Gaps in the record (time periods not represented by deposition) can potentially be
39
40 940 interpreted meaningfully as periods of relatively high precipitation and/or low
41
42 941 windspeed. Confidence in such interpretations grows if the gaps remain open in the
43
44 942 face of additional data, but such interpretations remain provisional in the absence of
45
46 943 independent verification.
47
48
49
50 944 • A new data treatment method (Accumulation Rate Variability, ARV) provides an
51
52 945 efficient proxy for changes in accumulation rate, hence aeolian activity, with
53
54 946 significant improvements over often-used date frequency methods. Using this
55
56 947 method, and in contrast to previous conclusions (Telfer *et al.*, 2010), we find
57
58 948 relatively small numbers of dated cores may be sufficient to accurately identify
59
60 949 multiple forcing events in some cases.

- An asymmetry exists between the efficiency of identifying dry events in wet periods (more likely) and wet events in dry periods (less likely), which relates to the time-separation of depositional periods and the correct distinction between hiatuses due to forcing conditions and those due to under-sampling.
- The effect of random errors (uncertainty) in dating imposes a filtering-out of higher frequency events, which increases with age, giving potentially false impressions that past changes in forcing occurred less frequently.
- The filtering-out of information on primary forcing conditions, through geomorphological processes, sampling and dating, no doubt makes the accurate interpretation of dune records more difficult. Although the details change, this problem is a general one, present in all attempts to understand the timing and nature of past events, whatever the proxies and whatever the dating methods employed. More explicit discussion of these issues can only serve to improve the quality and reliability of these endeavours.

Acknowledgements

Dr Giles Wiggs is thanked for helpful discussion of aeolian processes and windspeed distributions in desert environments during the development of the model. Other members of the Luminescence Dating Laboratory and Landscape Dynamics group at Oxford, particularly Dr Sallie Burrough, Dr Abi Stone and Carly Leighton, are thanked for their contributions to wide ranging and longstanding discussion about dating dryland sedimentary deposits using OSL. We thank anonymous referees for comments that have improved the paper, especially with regard to debates about stratigraphic completeness.

1
2
3
4
5
6
7
8
9
10
11
12
13
14
15
16
17
18
19
20
21
22
23
24
25
26
27
28
29
30
31
32
33
34
35
36
37
38
39
40
41
42
43
44
45
46
47
48
49
50
51
52
53
54
55
56
57
58
59
60

References

976
977
978 Anders MH, Krueger SW, Sadler PM. 1987. A new look at sedimentation rates and the
979 completeness of the stratigraphic record. *Journal of Geology* **95**: 1–14.
980
981 Atkinson OAC, Thomas DSG, Goudie AS, Parker A. 2012. Holocene development of
982 multiple dune generations in the northeast Rub’ al-Khali, United Arab Emirates. *The*
983 *Holocene* **22**: 179-189.
984
985 Barrell J. 1917. Rhythms and the measurement of geologic time. *Bulletin, Geological*
986 *Society of America* **28**: 745-904.
987
988 Bullard JE, Thomas DSG, Livingstone I, Wiggs GFS. 1996. Wind energy variations in
989 the Southwestern Kalahari desert and implications for linear dunefield activity. *Earth*
990 *Surface Processes and Landforms* **21**: 263-278.
991
992 Chase B. 2009. Evaluating the use of dune sediments as a proxy for palaeo-aridity: A
993 southern African case study. *Earth-Science Reviews* **93**: 31-45.
994
995 Chase BM, Thomas DSG. 2006. Late Quaternary dune accumulation along the western
996 margin of South Africa: distinguishing forcing mechanisms through the analysis of
997 migratory dune forms. *Earth and Planetary Science Letters* **251**: 318–333.
998
999 Cohen TJ, Nanson GC, Larsen JR, Jones BG, Price DM, Coleman M, Pietsch TJ. 2010.
1000 Late Quaternary aeolian and fluvial interactions on the Cooper Creek Fan and the

- 1
2
3
4 1001 association between linear and source-bordering dunes, Strzelecki Desert, Australia.
5
6 1002 *Quaternary Science Reviews* **29**: 455-471.
7
8 1003
9
10
11 1004 Dong Z, Liu X, Wang H, Wang X. 2003. Aeolian sand transport: a wind tunnel model.
12
13 1005 *Sedimentary Geology* **161**: 71–83.
14
15 1006
16
17
18 1007 Flint RF, Bond G. 1968. Pleistocene sand ridges and pans in western Rhodesia.
19
20 1008 *Bulletin of the Geological Society of America* **79**: 299–314.
21
22 1009
23
24
25 1010 Flores-Aqueveque V, Alfaro SC, Caquineau S, Foret G, Vargas G, Rutllant JA. 2012.
26
27 1011 Inter-annual variability of southerly winds in a coastal area of the Atacama Desert:
28
29 1012 Implications for the export of aeolian sediments to the adjacent marine environment.
30
31 1013 *Sedimentology* **59**: 990-1000.
32
33 1014
34
35
36 1015 Fryberger SG. 1979. Dune Form and Wind Regime. *US Geological Survey Professional*
37
38 1016 *Paper 1052*. US Geological Survey: Reston, VA: 137–169.
39
40 1017
41
42
43 1018 Goudie AS, 2002. Great warm deserts of the world. Oxford: Oxford University Press.
44
45 1019
46
47
48 1020 Hesse P. 2011. Sticky dunes in a wet desert: Formation, stabilisation and modification
49
50 1021 of the Australian desert dunefields. *Geomorphology* **134**: 309-325.
51
52 1022
53
54
55 1023 Hesse PP, Humphreys GS, Selkirk PM, Adamson DA, Gore DB, Nobes DC, Price DM,
56
57 1024 Schwenninger J-L, Smith B, Tulau M, Hemmings F. 2003. Late Quaternary aeolian
58
59 1025 dunes on the presently humid Blue Mountains, Eastern Australia. *Quaternary*
60
1026 *International* **108**: 13-32.

- 1027
- 1028 Hulme M. 1996. Recent climate changes in the world's drylands. *Geophysical Research*
- 1029 *Letters* **23**, 61-64.
- 1030
- 1031 Kemp DB. 2012. Stochastic and deterministic controls on stratigraphic completeness
- 1032 and fidelity. *International Journal of Earth Sciences (Geologische Rundschau)* **101**:
- 1033 2225–2238.
- 1034
- 1035 Kocurek G, Lancaster N. 1999. Aeolian system sediment state: Theory and Mojave
- 1036 Desert Kelso dune field example. *Sedimentology* **46**: 505-515.
- 1037
- 1038 Kocurek G. 1998. Aeolian system response to external forcing factors – a sequence
- 1039 stratigraphic view of the Saharan region. In *Quaternary Deserts and Climatic Change*
- 1040 Alsharan A, Glennie K, Whittle G, Kendall C (eds). Balkema: Rotterdam; 327–337.
- 1041
- 1042 Leighton CL, Bailey RM, Thomas DSG. (in press) The utility of desert sand dunes as
- 1043 Quaternary chronostratigraphic archives: Evidence from the northeast Rub' al Khali.
- 1044 *Quaternary Science Reviews*.
- 1045
- 1046 Leighton CL, Bailey, RM, Thomas DSG, Reproducibility and utility of dune
- 1047 luminescence chronologies (submitted, *Earth-Science Reviews*).
- 1048
- 1049 Lomax J, Hilgers A, Radtke U. 2011. Palaeoenvironmental change recorded in the
- 1050 palaeodunefields of the western Murray Basin, South Australia – new data from single
- 1051 grain OSL-dating. *Quaternary Science Reviews* **30**: 723–736.
- 1052

- McFarlane MJ, Eckardt FD, Ringrose S, Coetzee SH, Kuhn JR. 2005. Degradation of linear dunes in northwest Ngamiland, Botswana and the implications for luminescence dating of periods of aridity. *Quaternary International* **135**: 83–90.
- Merzouk NK. 2000. Wind energy potential of Algeria. *Renewable Energy* **21**: 553–562.
- Munyikwa K. 2005. The role of dune morphogenetic history in the interpretation of linear dune luminescence chronologies: a review of linear dune dynamics. *Progress in Physical Geography* **29**: 317–336.
- O. Durán, P. Claudin, B. Andreotti. 2011. On aeolian transport: Grain-scale interactions, dynamical mechanisms and scaling laws. *Aeolian Research* **3**: 243–270.
- O'Connor PW, Thomas DSG. 1999. The timing and environmental significance of late Quaternary linear dune development in western Zambia. *Quaternary Research* **52**: 44–55.
- Page KJ, Dare-Edwards AJ, Owens JW, Frazier PS, Kellett J, Price, D.M. 2001. TL chronology and stratigraphy of riverine source bordering sand dunes near Wagga Wagga, New South Wales, Australia. *Quaternary International* **82–85**: 187–193.
- Preusser F. 2009. Chronology of the impact of Quaternary climate change on continental environments in the Arabian Peninsula. *Comptes Rendus - Geoscience* **341**: 621–632.

- 1
2
3
4 1078 Reineck H-E. 1960. Über Zeitlücken in rezenten Flachsee-Sedimenten. *Geologische*
5
6 1079 *Rundschau* **49**:149–161.
7
8 1080
9
10
11 1081 Sadler PM. 1981. Sediment accumulation rates and the completeness of stratigraphic
12
13 1082 sections. *Journal of Geology* **89**: 569–584.
14
15 1083
16
17 1084 Sadler PM, Strauss DJ. 1990. Estimation of completeness of stratigraphical sections
18
19 1085 using empirical data and theoretical models. *Journal of the Geological Society of*
20
21 1086 *London* **147**: 471–485.
22
23
24 1087
25
26 1088 Singhvi AK, Porat N. 2008. Impact of luminescence dating on geomorphological and
27
28 1089 palaeoclimate research in drylands. *Boreas* **37**: 536–558.
29
30
31 1090
32
33 1091 Stone AEC, Thomas DSG. 2008. Linear dune accumulation chronologies from the
34
35 1092 southwest Kalahari, Namibia: challenges of reconstructing late Quaternary
36
37 1093 palaeoenvironments from aeolian landforms. *Quaternary Science Reviews* **27**: 1667–
38
39 1094 1681.
40
41
42 1095
43
44
45 1096 Telfer MW, Bailey RM, Burrough SL, Stone AES, Thomas DSG, Wiggs GFS. 2010.
46
47 1097 Understanding linear dune chronologies: insights from a simple accumulation model.
48
49 1098 *Geomorphology* **120**: 195–208.
50
51
52 1099
53
54 1100 Telfer M, Thomas DSG. 2007. Late Quaternary linear dune accumulation and
55
56 1101 chronostratigraphy of the southwestern Kalahari: implications for aeolian palaeoclimatic
57
58 1102 reconstructions and predictions of future dynamics. *Quaternary Science Reviews* **26**:
59
60 1103 2617–2630.

- 1104
- 1105 Telfer MW. 2011. Growth by extension, and reworking, of a south-western Kalahari
- 1106 linear dune. *Earth Surface Processes and Landforms* **36**: 1125-1135.
- 1107
- 1108 Thomas DSG. 2011. Arid environments: their nature and extent. In *Arid Zone*
- 1109 *Geomorphology*, Thomas DSG (ed). Chichester: Wiley; 3-16.
- 1110
- 1111 Thomas DSG. 2013. Reconstructing paleoenvironments and palaeoclimates in
- 1112 drylands: what can landform analysis contribute? *Earth Surface Processes and*
- 1113 *Landforms* **38**: 3–16.
- 1114
- 1115 Thomas, DSG, Burrough SL. 2012. Interpreting geo-proxies of late Quaternary climate
- 1116 change in African drylands: implications for understanding environmental and early
- 1117 human behaviour. *Quaternary International* **253**: 5-17.
- 1118
- 1119 Thomas DSG, Shaw PA. 1991. The Kalahari Environment. CUP, Cambridge.
- 1120
- 1121 Thomas DSG, Knight M, Wiggs GFS. 2005. Remobilization of southern African desert
- 1122 dune systems by twenty-first century global warming. *Nature* **435**, 1218-1221.
- 1123
- 1124 Tipper JC. 1983. Rates of sedimentation, and stratigraphic completeness. *Nature* **302**:
- 1125 696–698.
- 1126
- 1127 UNEP 1998. World atlas of desertification (2nd edition). London: Arnold.
- 1128

1
2
3
4
5
6
7
8
9
10
11
12
13
14
15
16
17
18
19
20
21
22
23
24
25
26
27
28
29
30
31
32
33
34
35
36
37
38
39
40
41
42
43
44
45
46
47
48
49
50
51
52
53
54
55
56
57
58
59
60

1129 Wiggs GFS, 2011. Sediment mobilisation by the wind. In *Arid Zone Geomorphology*,
1130 Thomas DSG (ed). Chichester: Wiley; 455-486.
1131
1132 Wiggs GFS, Thomas DSG, Bullard JE, Livingstone I. 1995. Dune mobility and
1133 vegetation cover in the southwest Kalahari Desert. *Earth Surface Processes &*
1134 *Landforms* **20**: 515-529.
1135
1136 Wolfe SA, Nickling WG. 1993. The protective role of sparse vegetation in wind erosion.
1137 *Progress in Physical Geography* **17**: 50-68.
1138
1139 Zhang G-P, Liu J-Y, Zhang Z-X, Zhao X-L, Zhou Q-B. 2002. Analysis of wind erosion
1140 caused landscape change and its relation with spatial distribution of wind energy. *Acta*
1141 *Geographica Sinica* **57**: 1-10.

Figure captions

Figure 1

A representation of the 'filtering' process, whereby information on past forcing conditions is progressively lost from the stratigraphic record. Thick-walled boxes draw attention to the processes which can, to some extent, be controlled. The information referred to is the description of climate and environmental forcing conditions, which is variously lost, modified and degraded by natural and investigative processes. That is, the ability to reconstruct the forcing conditions accurately is reduced by the processes listed.

Figure 2

The main figure shows the dependence of sediment flux on windspeed, calculated according to Equation 1, for grain size equal to 150, 200 and 250 μm (200 μm is used for all subsequent calculations). Grain size affects the threshold velocity for entrainment, and relevant data (from Dong *et al.*, 2003) are shown in the inset.

Figure 3

(i) Three different Weibull distributions (see main text for details), representing example windspeed distributions for 'low' ($k=2$), 'medium' ($k=3.5$) and 'high' ($k=5$) wind energy regimes (for reference, the vertical dashed line indicates the entrainment threshold velocity for 200 μm grains, 6.4 m/s). Applying these wind regimes for a period of one year to Equation 1 (randomly sampling the distributions for a years worth of seconds) results in the sand transport distributions shown in (ii) (plotted as duration (s per bin width of 0.0005Q, the resolution of the horizontal axis) against Q (per yr). (iii) The relationship between the parameter k (the 'shape factor' of the Weibull distribution) and

the ‘effective windspeed’ (u_{eff}) described in the main text. The dashed horizontal line shows the threshold velocity for entrainment. The Gaussian curve represents the distribution of the effective windspeed distribution (7 ± 1 m/s) used for many of the subsequent simulations.

Figure 4

(i) The inferred relationship between the effectiveness of aeolian transport and mean annual rainfall, as discussed in the main text. Parameters p_0 and p_1 set the precipitation values below which aeolian activity is unimpeded (p_0) and above which aeolian activity stops (p_1). (ii) The calculated combined effects of windspeed and precipitation on sand flux (calculated using Equation 5) note that transport falls to zero when windspeed is less than the entrainment velocity (6.4 m/s) and when precipitation exceeds p_1 (500 mm/yr).

Figure 5

(i) A cartoon of an idealized traverse dune, moving left to right, with wind direction, at three snapshots in time, t_1 - t_3 . The hypothesized net surface mass balance at each location (a-f) is indicated. See main text for further discussion. (ii) An example time series of ε , which controls the magnitude and duration of erosion and deposition in the model. A full description of how ε is generated, and how this affects model behaviour, is given in the main text.

Figure 6

The model response to a simplified forcing under conditions of constant maximum deposition ($\varepsilon=1$) and constant maximum erosion ($\varepsilon=-1$), as determined by windspeed and precipitation. (i) The windspeed and precipitation forcing. (ii) Surface height

(relative to the initial height) for both cases, of extreme erosion and deposition, and this is plotted also as an accumulation rate (for $\varepsilon=1$). (iii) The stratigraphic (age/depth) record which results from the simulation with $\varepsilon=1$.

Figure 7

Data equivalent to the plots in Figure 6, but with mean forcing conditions (effective windspeed and annual precipitation) constant and with the inclusion of a random 'noise' component (the standard deviations of the effective windspeed and annual precipitation are 1.5 m/s and 100 mm/yr respectively; see main text for details). The bold points in (i) identify the deposited sediment which survives subsequent periods of erosion. The accumulation rates calculated (for each model year) are shown in (ii) and the resulting age/depth profile is shown in (iii). Note the correspondence between (iii) and (i) and that, in this particular example, only approximately half of the duration of the simulation is represented in the age/depth profile.

Figure 8

The main plot shows the mean annual accumulation rate versus sediment age (time progresses from right to left), under conditions of constant mean effective windspeed and precipitation (where $\mu_{ueff}=7$, $\sigma_{ueff}=1.5$, $\mu_p=300$, $\sigma_p=150$). A smoothed version of the data is also shown, in bold, to highlight the main trend. The inset shows the same (smoothed) data on logarithmic scales, with a fit to the period 0.4-10 ka of the form $y=ax^b$, where $a=0.868 (\pm 0.027)$ and $b=-0.509 (\pm 0.04)$, discussed in the main text.

Figure 9

(i) The forcing conditions for Experiment 2. The variability in forcing is indicated over the initial 100 year interval; for clarity, only the mean values (the mean of the Gaussian

distributions from which values of precipitation and effective windspeed were taken) are shown after the first 100 yr. The standard deviations of the effective windspeed and annual precipitation are 1.5 m/s and 100 mm/yr respectively. The resultant accumulation (averaged over 1,000 model runs) is shown in (ii). (iii) and (iv) show equivalent data for Experiments 3. For experiment 2 and 3, the different sets of forcing conditions are referred to as case A-E, as shown, and these are explained in the main text. Vertical dashed lines are included to aid visual comparison.

Figure 10

(i) Changes in external sediment input (s , the dimensionless coefficient described in the main text) over time for Experiment 4. (ii) The resultant potential accumulation for the two extreme s_{max} values used in Experiment 4. For the case of $s_{max}=0.5$ the sediment response mirrors the forcing and is intermediate between $s_{max}=0.1$ and $s_{max}=1.0$ (not shown, to avoid overlapping data points). In (iii) the values of s are not plotted against either vertical axis, for graphical convenience, and indicative (extreme) values are shown in the figure. The standard deviations of the effective windspeed and annual precipitation are 1.5 m/s and 100 mm/yr respectively. The different sets of forcing conditions are labelled as cases I and J, as shown, and these are explained in the main text. Vertical dashed lines are included to aid visual comparison.

Figure 11

Age versus depth data from six repeats of Experiment 5 are plotted (parts (i) to (iv)). As shown, sampling resolution is 0.5 m and the error bars on each date represent the applied random uncertainty (see main text for details). Effective windspeed was sampled randomly from a Gaussian distribution ($\mu_{ueff}=7$) and mean precipitation changes through the simulation, as indicated by the plot in the lower right panel. The

standard deviations of the effective windspeed and annual precipitation are 1.5 m/s and 100 mm/yr respectively. The dashed lines demarcate the period in which precipitation is sufficiently high to modify sediment flux ($\mu_p > p_0$) and continuous lines indicate the period where sediment mobility ceases ($\mu_p > p_1$) (Equation 5). These are included to aid interpretation of the dates, and specifically to identify the gap in dates associated with peak precipitation.

Figure 12

The effect of random errors on the ability to distinguish depositional events. Full description of relevant calculations is given in the main text. (i) shows 90% and 50% 'success' contours, indicating the probability of distinguishing older/younger samples (assuming a relative dating precision of 8%). An example is shown to illustrate this: for a (younger) sample with a true age (t_1) of 70 ka, an older sample must have a true age (t_2) of 95 ka in order that the probability of identifying an age difference is 90%; similarly where the older sample is 70 ka, the younger sample must have a true age of 52 ka in order to be chronologically distinguishable (with a 90% chance of success). The main part of (ii) shows the age difference between resolvable ages, for different levels of dating precision. For example, with 10% dating precision, the minimum resolvable gap (with 90% change of success) at an age of 80 ka is 30 ka (see main text for details).

Figure 13

These plots are fully described in the main text (Experiment 6). The lowest data series in both parts (square waves) represent annual precipitation. In both cases, precipitation takes on either a lower value (100 mm/yr) or an upper value (600 mm/yr). The standard deviations of the effective windspeed and annual precipitation are 1.5 m/s and 100 mm/yr respectively. The value of N refers to the number of (virtual) cores used in the

1
2
3
4
5
6
7
8
9
10
11
12
13
14
15
16
17
18
19
20
21
22
23
24
25
26
27
28
29
30
31
32
33
34
35
36
37
38
39
40
41
42
43
44
45
46
47
48
49
50
51
52
53
54
55
56
57
58
59
60

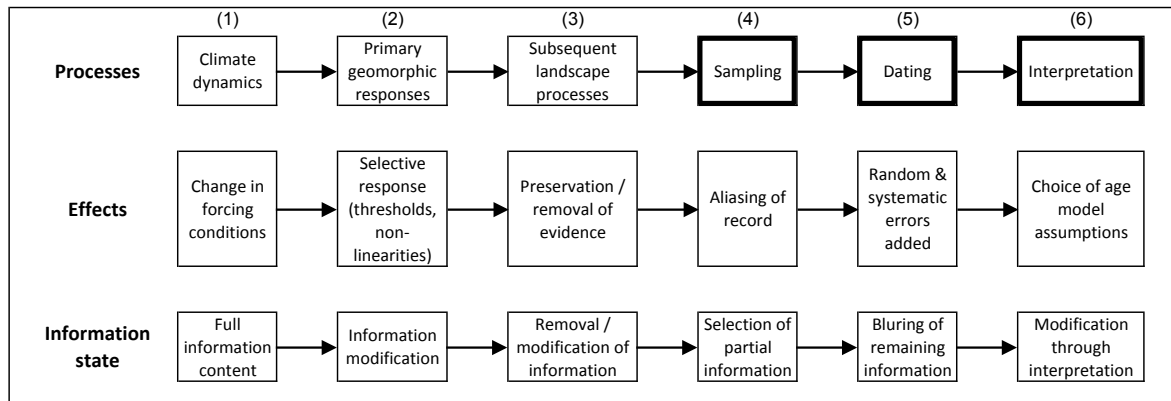
analysis. The error bars on the upper two data series in both parts are standard deviations, of all values within 100 year intervals.

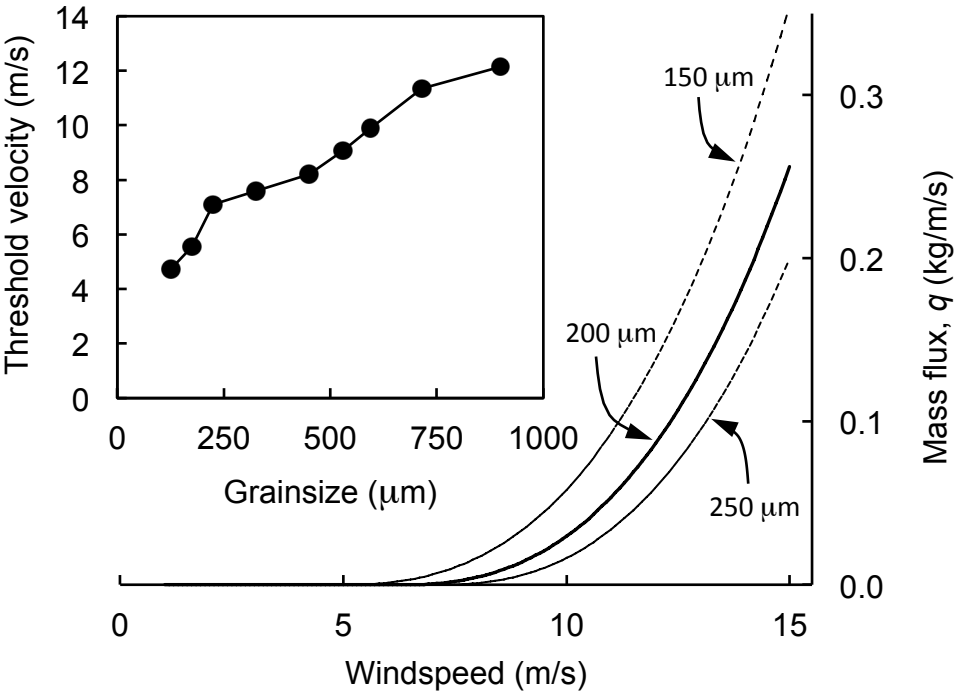
Figure 14

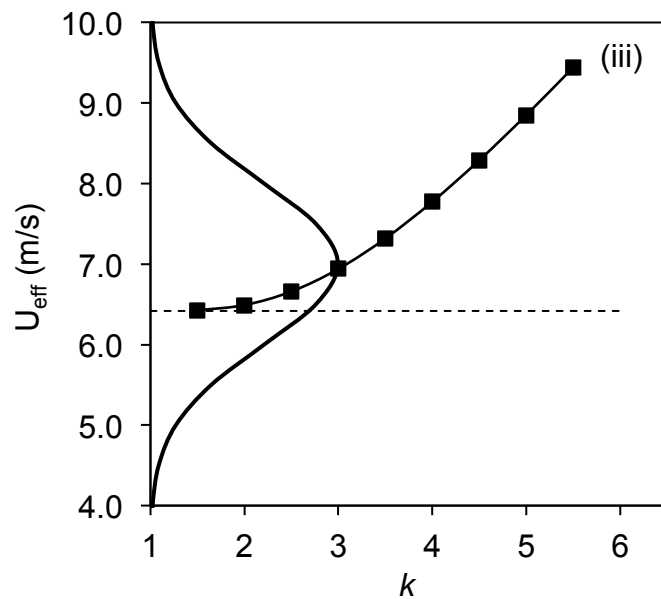
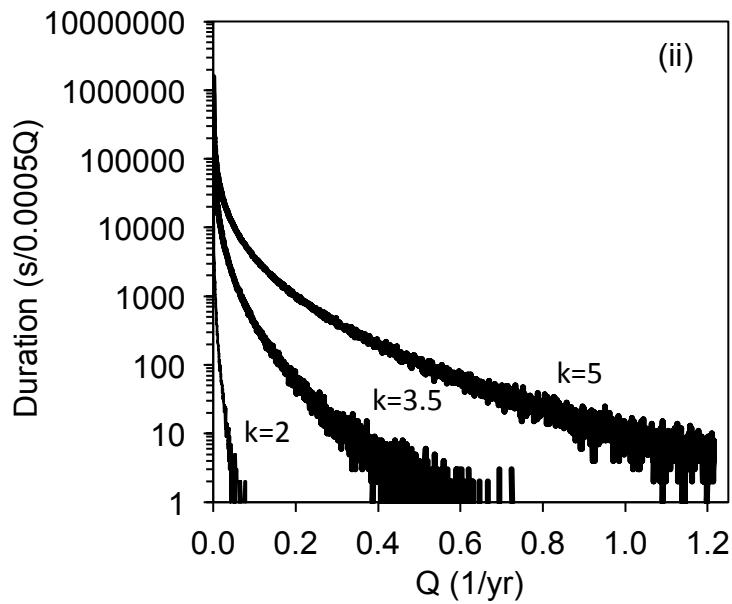
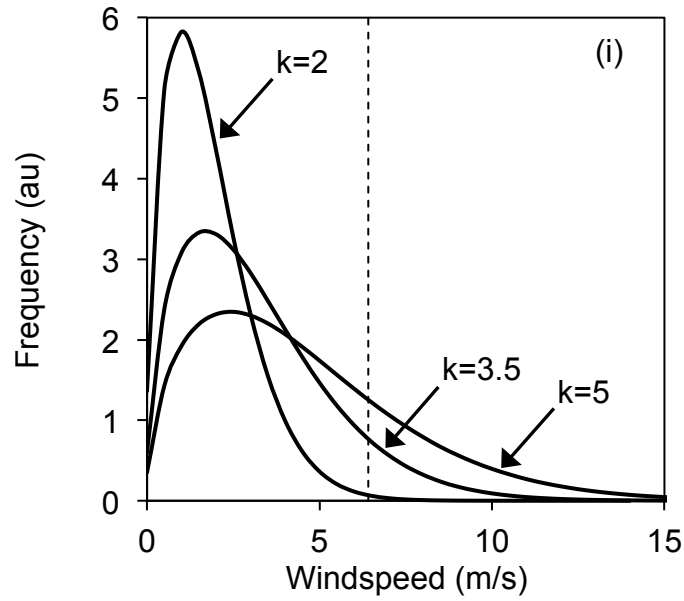
Data from Experiment 6 are presented as age estimates, in rank order. Values of n refer to the number of cores used in the analysis. The change in precipitation through time (between lower values of 100 mm/yr and upper values of 600 mm/yr) is indicated in (i). The standard deviations of the effective windspeed and annual precipitation are 1.5 m/s and 100 mm/yr respectively. The solid vertical bars indicate the time periods represented by the dates (at 1 sigma). Further detail and discussion is given in the main text.

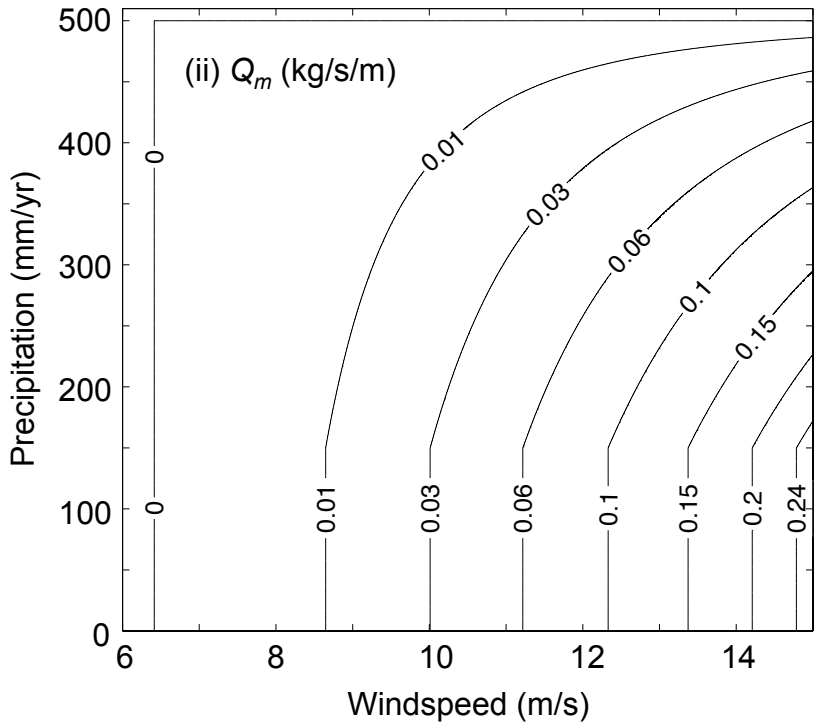
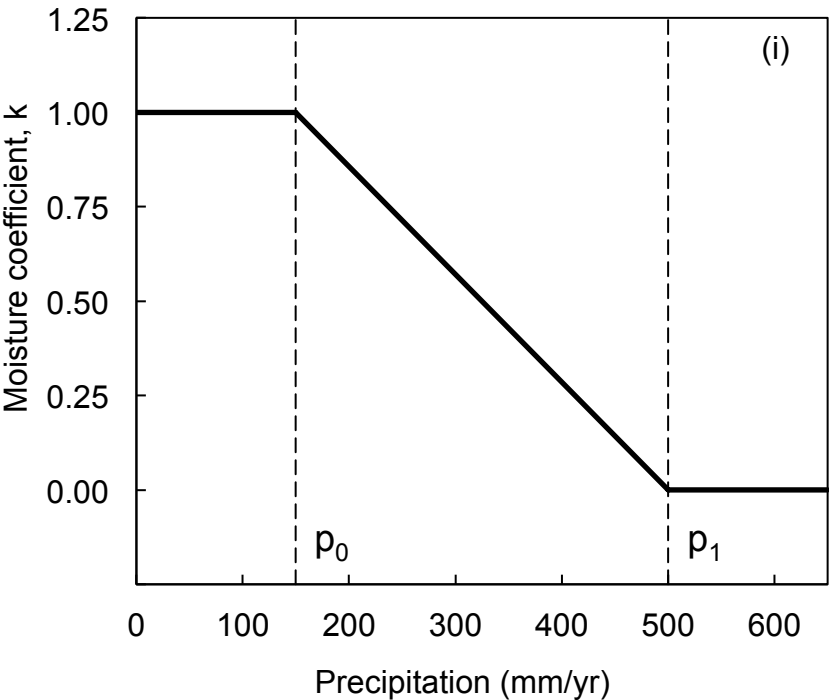
Figure 15

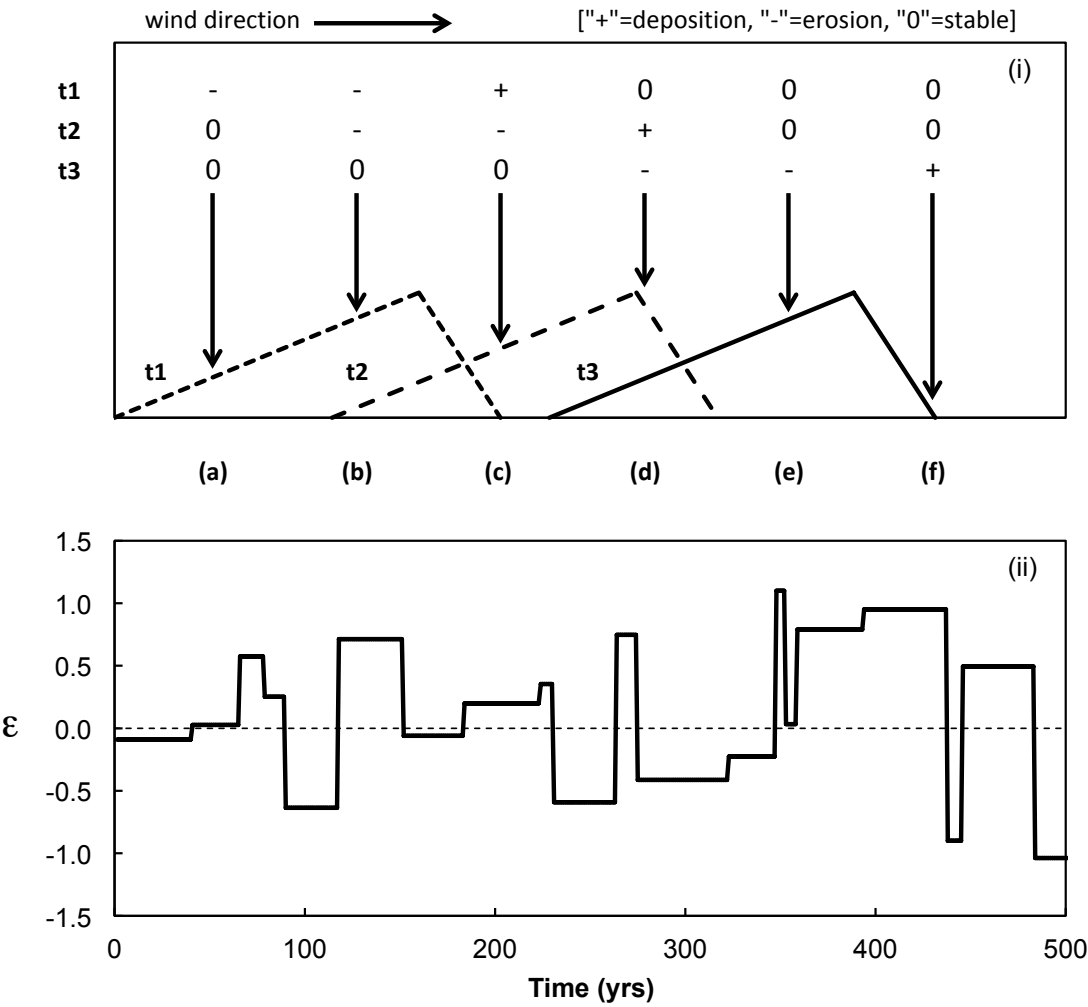
Data from Experiment 6 are shown. In each part, the upper data series is mean (\pm standard deviation) age frequency; the dashed and continuous lines show calculated ARV (see main text for explanation), for Experiment 6a (labelled [100,600], reflecting extremes of mean annual precipitation) and for Experiment 6c (labelled [200,400]). The lower (square) data set indicates precipitation extremes. The standard deviations of the effective windspeed and annual precipitation are 1.5 m/s and 100 mm/yr respectively. Further detail and discussion is given in the main text.











1
2
3
4
5
6
7
8
9
10
11
12
13
14
15
16
17
18
19
20
21
22
23
24
25
26
27
28
29
30
31
32
33
34
35
36
37
38
39
40
41
42
43
44
45
46
47
48
49
50
51
52
53
54
55
56
57
58
59
60

